



Cite this: *Green Chem.*, 2015, **17**, 1204

Synergistic effects of Ni and acid sites for hydrogenation and C–O bond cleavage of substituted phenols

Wenji Song,^a Yuanshuai Liu,^a Eszter Baráth,^a Chen Zhao*^{†a} and Johannes A. Lercher*^{a,b}

The cleavage of C–O bonds in phenol, catechol, and guaiacol has been explored with mono- and dual-functional catalysts containing Ni and/or HZSM-5 in the aqueous phase. The aromatic ring of phenol is hydrogenated in the first step, and the C–O bond of the resulting cyclohexanol is dehydrated in sequence. The initial turnover frequency (TOF) of phenol hydrodeoxygenation increases in parallel with the acid site concentration irrespective of the concentration of the accessible surface Ni atoms. For catechol and guaiacol conversion, Ni catalyzes the hydrogenolysis of the C–O bonds in addition to arene hydrogenation. For catechol, the hydrogenation of the aromatic ring and the hydrogenolysis of the phenolic –OH group occur in parallel with a ratio of 8 : 1. The saturated cyclohexane-1,2-diol can be further dehydrated over HZSM-5 or hydrogenolyzed on Ni to complete hydrodeoxygenation. Guaiacol undergoes primarily hydrogenolysis (75%) to phenol *via* demethoxylation, and the hydrogenation route accounts for only 25%. This is attributed to the steric effects arising from the adjacent sp³ hybrid O–CH₃ group. 2-Methoxycyclohexanol (from guaiacol hydrogenation) reacts further either *via* hydrogenolysis by Ni to cyclohexanol or *via* acid catalyzed demethoxylation and rearrangement steps followed by the subsequent hydrogenation of the intermediately formed olefins. On Ni/HZSM-5, the hydrodeoxygenation activities are much higher for the phenolic monomers than for their respective saturated analogues, pointing to the importance of sp² orbitals. The presence of proximal acid sites increases the activities of Ni in the presence of H₂ by a synergistic action.

Received 17th September 2014,
Accepted 10th November 2014
DOI: 10.1039/c4gc01798f

www.rsc.org/greenchem

1. Introduction

Lignin is an abundant biopolymer composed of substituted C₉ propyl-phenol units, which are randomly cross-linked by C–C and C–O bonds.¹ Bio-oil derived from liquefaction or pyrolysis of lignin is seen as a promising source for second-generation bio-derived energy carriers.² However, the direct application of bio-oil is limited by its poor volatility, high viscosity, as well as its low stability caused by high contents of oxo-functionalized compounds.³ In this context, hydrodeoxygenation (HDO) is considered as the most effective method for converting oxygen-rich lignin derived bio-oil to clean oxygen-free hydrocarbon fuels.⁴

Lignin derived bio-oil comprises of a wide variety of C_{aryl}–OH, C_{aryl}–OCH₃, and C_{alkyl}–OR as well as C=O bonds. Cleavage of the C=O double bond requires stepwise hydrogenation and dehydration, whereas the former three types of C–O single bonds can be directly cleaved by metal-catalyzed hydrogenolysis. Alternatively, acid sites also catalyze the cleavage of C_{aryl}–OR and C_{alkyl}–OR bonds through hydrolysis. The formed C_{alkyl}–OH bond can be eliminated *via* dehydration. Removing oxygen in the C_{aryl}–OH bond, however, involves cascade reactions of hydrogenation and dehydration. The bond dissociation energies of C_{aryl}–O bonds are around 80–100 kJ mol^{−1} higher than those of C_{alkyl}–O bonds;^{4,5} while on the other hand, the steric constraints of cleaving C_{alkyl}–O bonds are much higher than for C_{aryl}–O bonds. Thus, it is highly important to understand the integrated steps of hydrogenolysis, hydrogenation, hydrolysis, and dehydration, to efficiently cleave the various C–O bonds in phenol derivatives.

In the past, sulfide-based hydrotreating catalysts have been employed for the hydrodeoxygenation of functionalized phenols.⁶ For instance, in the gas phase guaiacol was reported to be first converted *via* hydrogenolysis of the methoxy group

^aDepartment of Chemistry and Catalysis Research Center, Technische Universität München, Lichtenbergstraße 4, 85747 Garching, Germany.
E-mail: czhao@chem.ecnu.edu.cn

^bInstitute for Integrated Catalysis, Pacific Northwest National Laboratory, 902 Battelle Boulevard Richland WA 99352 USA. E-mail: johannes.lercher@ch.tum.de
†Current address: Shanghai Key Laboratory of Green Chemistry and Chemical Process, Department of Chemistry, East China Normal University, North Zhongshan Road 3663, 200062 Shanghai, China.

to catechol and methane, followed by hydrogenolysis of the hydroxyl group of catechol to phenol, which in turn was deoxygenated by hydrogenolysis and hydrogenation forming benzene, cyclohexene, and cyclohexane.⁷ Severe coke formation was observed during the conversion of both guaiacol and catechol with Al₂O₃ supported NiMo- or CoMo-sulfides.^{7a,8} By comparison, using dual functional catalysts with metal/acid sites such as Pd/C and H₃PO₄, guaiacol was primarily hydrogenated to 2-methoxycyclohexanol in the aqueous phase, which was in turn hydrolyzed producing cyclohexane-1,2-diol followed by consecutive acid catalyzed dehydration and metal catalyzed hydrogenation leading to cyclohexane formation.⁹ Carbonaceous deposits were negligible for such an aqueous-phase catalytic process.

Recently, we have reported that Ni supported on zeolite HZSM-5 catalyzes quantitative hydrodeoxygenation of the *n*-hexane-soluble fraction of pyrolysis oil to C₅–C₉ hydrocarbons under mild conditions (523 K, 5 MPa H₂) in water.¹⁰ In this contribution, the synergistic roles of the metal and acid sites of Ni/HZSM-5 in the aqueous phase are explored, including the integrated hydrogenation and hydrogenolysis over Ni sites, as well as the dehydration and rearrangements with acid sites of HZSM-5. The kinetics of the conversions of phenolic monomers and of their respective saturated cyclic alcohols are described and discussed, in order to elucidate the difference of opening aliphatic and aromatic C–O bonds in phenols and alcohols. The positive influence of proximal acid sites on the Ni activities is also highlighted.

2. Experimental section

2.1 Chemicals

All chemicals were obtained from commercial suppliers and used as received. Phenol (Sigma-Aldrich, 99%), 1,2-hydroxylbenzene (Sigma-Aldrich, ≥99%), *cis*-cyclohexane-1,2-diol (Aldrich, 99%), 2-methoxyphenol (Sigma-Aldrich, oxidation indicator), (1*S*,2*S*)-(+)-2-methoxycyclohexanol (Alfa Aesar, 99%), ethyl acetate (Sigma-Aldrich, 99.9%), Ni(II) nitrate hexahydrate (Sigma-Aldrich, ≥98.5%), urea (Sigma-Aldrich, BioReagent). NH₄-ZSM-5 with framework Si/Al ratios of 11.5 and 25 were purchased from Zeolyst International, and HZSM-5 with Si/Al = 90 were obtained from Clariant. All three zeolites were calcined in air at 823 K for 6 h before usage.

2.2 Preparation of Ni/HZSM-5 catalysts

The deposition–precipitation (DP) method was applied to prepare the Ni based catalysts, according to procedures reported in the literature.¹¹ In a typical synthesis, 250 mL aqueous solution of Ni(NO₃)₂ (0.14 M) was prepared and divided into two parts. 210 mL of it was made into a suspension with 2 g parent HZSM-5 zeolite, and urea was dissolved in the rest 40 mL of the solution. The zeolite suspension was heated up to 343 K at which the urea solution was added dropwise, and then the mixture was brought up to 363 K to start the DP process. After 2 hours, the suspension was cooled to

ambient temperature, vacuum filtered, and then the solid was washed three times with double distilled water. The obtained samples were dried at 383 K in air overnight. The catalyst precursors were calcined at 673 K for 4 h in air with a heating rate of 1 K min^{−1} (flow rate: 100 mL min^{−1}), and then reduced in pure hydrogen at 733 K for 5 h with a heating rate of 1 K min^{−1} (hydrogen flow: 150 mL min^{−1}). The preparation of the Ni/SiO₂ catalyst followed similar procedures as described for Ni/HZSM-5, but with a DP duration of three hours.

2.3 Catalyst characterization

An elemental analysis of Ni contents in the catalyst samples was carried out by atomic absorption spectroscopy (AAS) on a UNICAM 939 AA-spectrometer. Prior to measurements, the sample was dissolved in a mixture of hydrofluoric acid (48%) and nitro-hydrochloric acid at its boiling point.

The BET specific surface area and pore volume were determined by N₂ adsorption–desorption isotherms measured at 77 K using a PMI automatic sorptometer. The catalyst was activated in a vacuum at 473 K for 2 h before the measurements. The specific surface areas were calculated by applying the Brunauer–Emmett–Teller (BET) theory, and the *t*-plot method was used to determine the pore volumes.¹²

Temperature programmed desorption (TPD) of NH₃ was performed in a 6-fold parallel reactor system. About 50 mg of each catalyst was loaded into individual reactors and activated in He at 773 K for 1 h (heating rate: 5 K min^{−1}). NH₃ was adsorbed with a partial pressure of 1 mbar at 373 K, and subsequently, the samples were purged with He (30 mL min^{−1}) for 2 h to remove physisorbed molecules. For the measurement of temperature programmed desorption, the catalyst samples were heated up in flowing He from 373 to 1033 K with a temperature increment of 10 K min^{−1} to desorb ammonia. The desorbed species (*m/z*⁺ = 16 signal) were monitored by mass spectrometry (Balzers QME 200). For acid site quantification, a reference (HZSM-5, Si/Al = 45 from Clariant) with known acidity was used to calibrate the signal.

The infrared spectra of adsorbed pyridine (Py-IR) were recorded with a Thermo Nicolet 5700 spectrometer at a resolution of 4 cm^{−1}. The sample was prepared as a self-supporting wafer and activated in a vacuum (*p* = 10^{−7} mbar) at 723 K for 1 h (heating rate = 10 K min^{−1}). After cooling to 423 K, the sample was equilibrated with 0.1 mbar of pyridine for 30 min, followed by outgassing for 1 h, and the IR spectra of chemisorbed pyridine were recorded subsequently. For quantification, molar integral extinction coefficients of 0.73 cm μmol^{−1} and 0.96 cm μmol^{−1} were used for the characteristic vibration bands of pyridinium ions and pyridine bound to Lewis acid sites, respectively.

Transmission electron microscopy (TEM) images were taken by a JEM-2010 Jeol transmission microscope operating at 120 kV. The catalyst sample was first suspended in ethanol by ultrasonication, and a drop of the suspension was deposited onto a carbon-coated Cu grid. More than 300 particles were counted to determine the average particle size.

The crystal structures of the catalyst powder were analyzed by X-ray diffraction (XRD) using a Philips X'Pert Pro System, with Cu-K α radiation operating at 45 kV/40 mA. The sample was measured with a scanning rate of 0.017° s⁻¹ in the range from 5 to 70° (2 θ). The metal particle size was calculated from the diffraction of Ni(111) by the Scherrer equation.

The IR spectra of the adsorbed CO were recorded on a Bruker Vertex 70 spectrometer at a resolution of 4 cm⁻¹ with 128 scans. The catalyst wafer was first reduced *in situ* in H₂ (1 bar) at 723 K for 1 h (heating rate = 10 K min⁻¹), and then the system was evacuated for 1 h ($p = 10^{-6}$ mbar). CO was adsorbed with an equilibrium pressure of 0.5 mbar at 313 K, followed by outgassing to remove the physically adsorbed CO. The IR spectra were recorded every five minutes until no changes in the spectra were observed. In order to directly compare the surface coverage of the adsorbed CO, each spectrum reported was normalized by the weight of the respective wafer. The IR spectra of the adsorbed phenol were measured with similar activation and adsorption procedures as described above, only that an equilibrium pressure of 0.05 mbar phenol was applied.

For measuring H₂ chemisorption, the Ni based catalyst was activated in vacuum at 588 K for 1 h and then cooled to ambient temperature. The H₂ adsorption isotherms accounting for both chemisorption and physisorption were measured in pressure ranging from 1 to 0.4 bar. Afterwards, the system was evacuated for 1 h to remove physisorbed H₂. The concentration of chemisorbed hydrogen on the metal was determined by extrapolating the isotherm to zero H₂ pressure. The Ni dispersion was deduced by assuming an average H/Ni ratio of 1.

2.4 Catalytic measurements

The kinetic study of the aqueous-phase hydrodeoxygenation (HDO) of phenol was carried out as follows: 1.0 g reactant, 0.02 g Ni based catalyst, and 100 mL distilled water were charged into a batch autoclave (Parr Instrument, 300 mL), and stirred at a speed of 700 rpm. The reactor was purged with 30 bar H₂ at ambient temperature, and then heated up to 473 K at which the reaction started. Since *in situ* sampling was difficult to carry out for the biphasic reaction, the conversion/selectivity as a function of reaction time reported herein was obtained from the analysis of separate batch reactions with varied lengths of reaction time.

For HDO of catechol and guaiacol, 0.05 g of the catalyst was applied. With the saturated alcohol reactants, *i.e.*, cyclohexane-1,2-diol and 2-methoxycyclohexanol, a reactant to catalyst ratio of 0.2 g/0.04 g was adapted due to their relatively low activities.

After each batch reaction, ethyl acetate was applied to extract the products in the organic phase. Both aqueous-phase and organic-phase products were analyzed by Shimadzu gas-chromatography mass-spectroscopy (GC-MS) equipped with a flame ionization detector (FID) and an HP-5 capillary column. Conversion = (weight of the converted reactant/weight of the starting reactant) \times 100%. Yield of liquid products (C%) = (C atoms in liquid products/C atoms in the starting reactant) \times

100%. Selectivity (C%) = (C atoms of each product/C atoms in all the liquid products) \times 100%.

3. Results and discussion

3.1 Catalyst characterization

The main physicochemical properties of the parent HZSM-5 and the Ni/HZSM-5 samples are compiled in Table 1. The Ni contents of the three Ni/HZSM-5 were comparable at 20 wt% determined by AAS. N₂ adsorption-desorption isotherms were nearly identical for the three HZSM-5, with the same micropore volumes of 0.17 cm³ g⁻¹, whereas for HZSM-5 with Si/Al of 11.5, the mesoporous surface area was notably lower than the other two samples, *i.e.*, 28 m² g⁻¹ as compared to 57 and 77 m² g⁻¹. Upon addition of Ni, the volume of micropores decreased (0.17 to 0.12 cm³ g⁻¹), indicating that a part of the Ni particles was located in the micropores.

The acidic properties of the catalysts and the parent zeolites were probed by the TPD of NH₃ and by the IR spectra of adsorbed pyridine (Py-IR) (Table 2). The two techniques showed excellent agreement in terms of total acid site concentrations (discrepancy < 5%). For Ni/HZSM-5 and the parent HZSM-5, the concentration of Brønsted acid sites decreased as expected with the increasing framework Si/Al ratio, *i.e.*, 0.93, 0.44, and 0.14 mmol g⁻¹ for HZSM-5 11.5, 25, and 90, respectively. After the deposition of Ni(II) salts, the concentrations of Brønsted acid sites decreased significantly to 0.38, 0.16, and 0.08 mmol g⁻¹. This is attributed to the hetero-condensation of the zeolite acidic hydroxyl groups with Ni(II) hydroxoqua

Table 1 Physicochemical properties of parent HZSM-5 and Ni/HZSM-5 samples

Catalyst	Si/Al ratio	BET surface area (m ² g ⁻¹)			Pore volume (cm ³ g ⁻¹)		
		Micro	Meso	Total	Micro	Meso	Total
HZSM-5	11.5	386	28	414	0.17	0.04	0.21
	25	381	57	438	0.17	0.08	0.25
	90	362	77	439	0.17	0.09	0.26
Ni/HZSM-5 (20 wt%)	11.5	261	30	291	0.12	0.05	0.17
	25	267	78	345	0.12	0.15	0.27
	90	232	114	346	0.11	0.15	0.26

Table 2 Acid characterization of parent HZSM-5 and Ni/HZSM-5 measured by TPD of NH₃ and IR spectra of adsorbed pyridine

Catalyst	Si/Al ratio	Acid sites determined Py-IR (mmol g ⁻¹)			TPD-NH ₃ (mmol g ⁻¹)
		Brønsted	Lewis	Total	
HZSM-5	11.5	0.93	0.15	1.07	1.07
	25	0.44	0.09	0.53	0.52
	90	0.14	0.01	0.15	0.14
Ni/HZSM-5 (20 wt%)	11.5	0.38	0.39	0.77	0.79
	25	0.16	0.18	0.34	0.37
	90	0.08	0.11	0.19	0.17

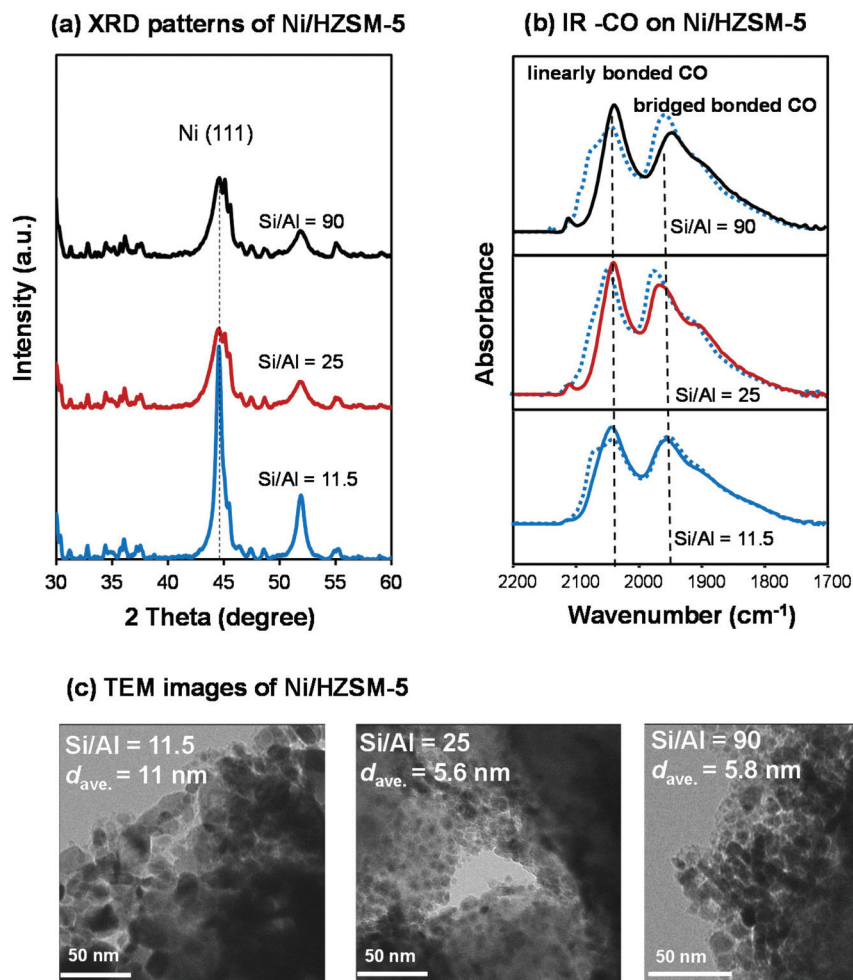


Fig. 1 Characterization of Ni/HZSM-5 with three Si/Al ratios by (a) XRD patterns, (b) IR spectra of adsorbed CO, with dotted lines: at 0.5 mbar of CO equilibrium pressure, and solid lines: after evacuation, (c) TEM images.

complexes during the DP process.¹³ In contrast, higher concentrations of Lewis acid sites were observed with Ni/HZSM-5 (0.39, 0.18, 0.11 mmol g⁻¹) compared to parent HZSM-5 (0.15, 0.09, 0.01 mmol g⁻¹) as the Si/Al ratio increased. These additional Lewis acid sites stem from the incompletely/un-reduced Ni cations, as confirmed for Ni/HBEA prepared by the DP method.¹⁴

XRD, TEM, and IR spectra of the adsorbed CO were applied to characterize the size, morphology, and accessible fraction of Ni atoms in Ni/HZSM-5 catalysts (Fig. 1). Based on the peak at the diffraction angle (2θ) of 44° (Fig. 1a), $d_{\text{Ni}(111)}$ was calculated according to the Scherrer equation to be 14, 5.2, and 6.5 nm (Table 3) for the supports with Si/Al ratios of 11.5, 25, 90,

respectively. Two pronounced bands of adsorbed CO after evacuation appeared at 2040–2045 cm⁻¹ and 1910–1970 cm⁻¹ in the IR spectra (Fig. 1b). The former is assigned to linearly adsorbed CO on Ni⁰, the latter corresponds to two or three fold bridged adsorption of CO on Ni⁰.¹⁵ The integral area under these two bands is proportional to the concentration of accessible Ni⁰ sites. Ni/HZSM-5 11.5 showed the smallest intensity of adsorbed CO, indicating that this sample had the lowest concentration of accessible Ni atoms. Hence, we conclude that the largest metal particles were formed on Ni/HZSM-5 11.5, in accordance with the results obtained from XRD diffractograms (see Table 3). This trend was also confirmed by TEM images (Fig. 1c), in which Ni/HZSM-5 11.5 showed the largest Ni particles with an average diameter of 11 nm, while the other two Ni/HZSM-5 samples displayed much smaller particles (5.6 and 5.8 nm).

Since all three Ni/HZSM-5 catalysts were prepared by the same deposition–precipitation method and the resulting Ni contents were nearly identical, the observed differences in the Ni particle sizes are tentatively related to differences during the preparation procedure induced by zeolite properties. As

Table 3 Ni size characterization of three Ni/HZSM-5 measured by TEM, XRD, and H₂ chemisorption

Si/Al ratio	d_{TEM} (nm)	$d_{\text{XRD Ni}(111)}$ (nm)	$D_{\text{H}_2 \text{ chem.}}$ (%)
11.5	11 ± 3.4	14	3.6
25	5.6 ± 1.9	5.2	7.2
90	5.8 ± 2.2	6.5	9.6

pH values of the three zeolite suspensions were measured to be comparable (4.2–4.5), variations in the aqueous phase environment during Ni(II) deposition can be excluded. Burattin *et al.* explored key parameters controlling the size of supported metal particles prepared by the deposition–precipitation method,¹⁶ including the nature of the deposited Ni(II) phase as well as the strength and extent of the metal–support interface. It was shown that the interface is manifested as a brucitic layer of octahedral Ni(II) bonding to the support surface, which provides anchoring sites for the overlying metal particles.^{16b} In the present case, the nature of the deposited Ni(II) phase in these catalysts is considered to be identical for all three samples due to the similar HZSM-5 supports and DP conditions. However, the lowest mesoporous area of HZSM-5 with the framework Si/Al ratio of 11.5 (Table 1) was speculated to lead to a less extended Ni–support interface, as observed in the literature for low surface area SiO₂.^{16a} In consequence, a relatively inhomogeneous Ni(II) phase was formed, leading to less uniformly distributed Ni nanoparticles. This trend agrees well with the observed drastic difference of Ni particle size and dispersion in the resulting catalyst samples.

In this contribution, Ni supported on neutral SiO₂ with a similar metal loading (20 wt%) as the zeolite supported ones was also investigated as a reference catalyst. The characterization results of Ni/SiO₂ are compiled in Fig. 2 and Table 4. N₂ sorption isotherm showed a specific surface area of 211 m² g⁻¹ and a pore volume of 0.52 cm³ g⁻¹. In particular, its mesoporous surface area (194 m² g⁻¹) was much larger than those of the three Ni/HZSM-5 catalysts (Table 1). The Ni particle size of Ni/SiO₂ was around 2.6 nm determined by XRD and TEM techniques (Fig. 2), and the metal dispersion was 20% analyzed by H₂ chemisorption. The much smaller Ni particles present in the SiO₂ supported catalyst again could be

related to its large mesoporous surface area as discussed above.

3.2 Hydrodeoxygenation of phenol

In order to explore the roles of acid and metal sites in the bifunctional Ni/HZSM-5 catalysts, the kinetics of hydrodeoxygenation of phenol (as the simplest model compound) were performed in the aqueous phase at 473 K (Fig. 3). The reaction proceeded in the similar pathway as proposed previously (Scheme 1).^{9,17} Phenol was first hydrogenated by Ni forming cyclohexanone as the primary product, which was gradually converted further to cyclohexanol. In the presence of Brønsted acid sites, cyclohexanol was dehydrated to cyclohexene, which was subsequently hydrogenated to cyclohexane. Therefore, the overall reaction pathway for the cleavage of the aryl C–O bond in phenol requires two catalyst functions, with Ni catalyzing the hydrogenation of the aromatic ring and alkene, and acid sites mediating the dehydration of cyclohexanol.

The rate of phenol hydrogenation on Ni is formally expressed as $r = k[\text{Phenol}]^a[\text{H}]^b$, where a and b denote the reaction order with respect to adsorbed phenol and H. In our case, the initial hydrodeoxygenation rates for the three Ni/HZSM-5 catalysts were comparable at 102, 88, and 84 mmol g⁻¹ h⁻¹ (Fig. 3a). Considering that the concentration of accessible Ni was very different (Table 3), we speculate that the concentrations of the adsorbed reactants are important properties determining the relative hydrogenation rates of this series of dual functional catalysts under selected conditions.

The concentration of phenol on Ni/HZSM-5 samples was estimated *via* the IR spectra of adsorbed phenol from the gas phase recorded after evacuation at 313 K (Fig. 4). Two bands at 1597 cm⁻¹ and 1495 cm⁻¹ are assigned to aromatic ring vibrations typical for the phenate species; whereas the

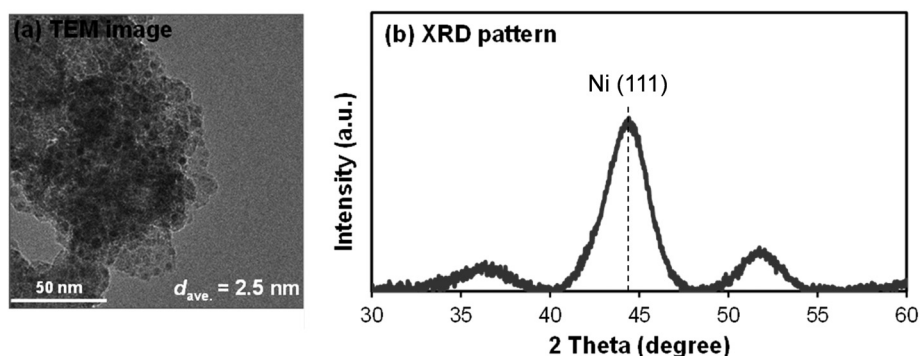


Fig. 2 (a) TEM image and (b) XRD pattern of Ni/SiO₂.

Table 4 Characterization of the Ni/SiO₂ catalyst

BET surface area (m ² g ⁻¹)			Pore volume (cm ³ g ⁻¹)			d_{TEM} (nm)	$d_{\text{XRD Ni(111)}}$ (nm)	$D_{\text{H}_2, \text{chem.}}$ (%)
Micro-	Meso-	Total	Micro-	Meso-	Total			
17	194	211	0.008	0.511	0.519	2.5 ± 0.5	2.7	20

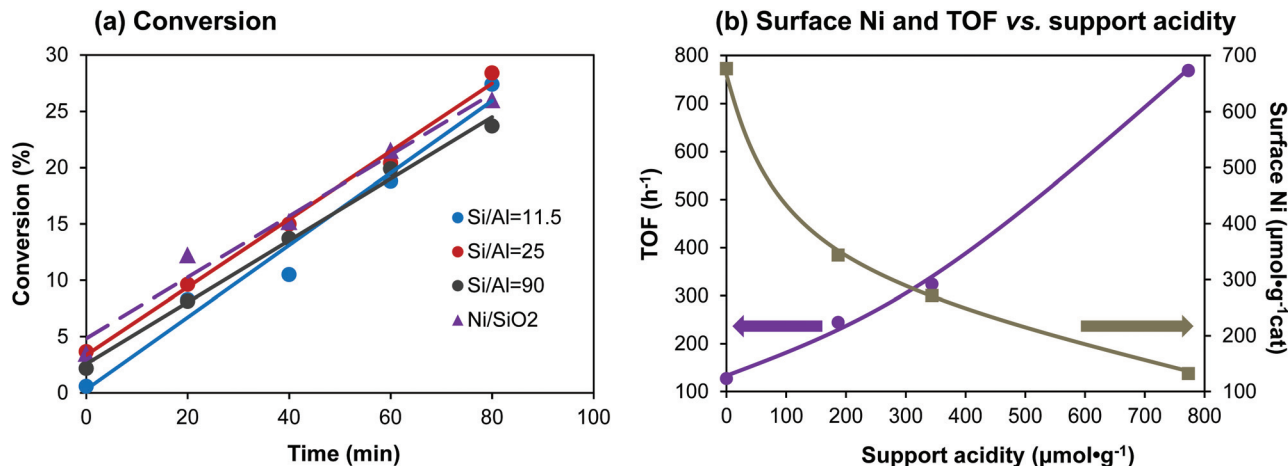
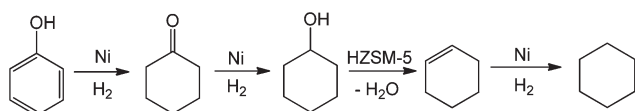


Fig. 3 Phenol hydrodeoxygenation on Ni based catalysts as a function of reaction time, (a) conversion, and (b) surface Ni atoms and turnover frequencies as a function of support acidity. Reaction conditions: 1.0 g phenol, 0.02 g catalyst, 473 K, 30 bar H₂ (ambient temperature), stirring at 700 rpm.



Scheme 1 Reaction pathway for phenol hydrodeoxygenation over Ni/HZSM-5 in the aqueous phase.

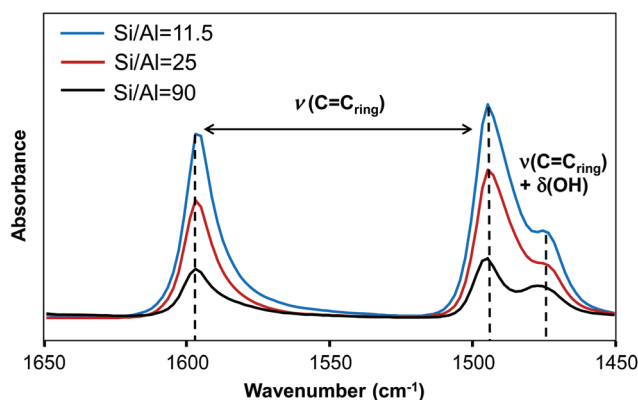


Fig. 4 IR spectra of adsorbed phenol on Ni/HZSM-5 after evacuation at 313 K.

shoulder at 1475 cm⁻¹ represents the C=C_{ring} vibration characteristic of H-bonded phenols, with contribution from the -OH group.¹⁸ The largest integral intensity was observed for Ni/HZSM-5 11.5 (Fig. 4), pointing to the highest phenol concentration on this catalyst. It should be noted that in the sole presence of Brønsted acid sites such as macroporous solid acids like Amberlyst or heteropoly acids, phenol hardly adsorbs from the gas phase.¹⁹ This implies that majority of the interaction results from strong dispersion forces upon physisorption of phenol in zeolite pores, as well as *via* its basic oxygen atom interacting with extra-lattice Al³⁺ cations, *i.e.*, the strong Lewis acid sites of zeolites. The formation of H-bonded

phenol originating from phenol interaction with SiOH groups or Brønsted acid sites in the zeolite cannot be fully excluded, as evidenced by the shoulder at ~1475 cm⁻¹,¹⁸ but such interactions of aromatic compounds with acid sites hardly contribute to the bonding.²⁰

When intrinsic rates of these series of Ni based catalysts were considered, the turnover frequencies (TOF) followed the order of Ni/HZSM-5 11.5 (769 h⁻¹) > Ni/HZSM-5 25 (324 h⁻¹) > Ni/HZSM-5 90 (244 h⁻¹) > Ni/SiO₂ (127 h⁻¹), which was in agreement with the decreasing Brønsted acid site concentrations of the respective supports (Fig. 3b). This suggests that apart from catalyzing cyclohexanol dehydration, the presence of support acidity also substantially enhances the rate of the phenol hydrogenation step, *i.e.*, with the increasing acid site concentration, the intrinsic hydrogenation rate increases accordingly.

Generally, the higher activities of noble metals (Pd or Pt) on acidic supports have been attributed in the past to modified adsorption properties and alteration of the metal band structure induced by proximal protons.²¹ Though several models have been proposed, the nature of the addressed metal-proton interaction as well as its direct impact on the catalytic activity remains unclear. We would like to involve, therefore, a different explanation. It has been well demonstrated²² that protonated pendant amine ligands when carefully positioned in organometallic complexes, enhance the rate of hydrogen oxidation or proton reduction by lowering free energy barriers for these catalytic reactions. The present case is speculated to resemble the effect of such molecular (electro)catalysis, in which the Brønsted acid site provides an additional delivery of the proton for the hydrogenation process.

By invoking such a cooperative action, the concentration of active H in the above addressed rate expression would not only be determined by the concentration of hydrogen adsorbed on the Ni particle, but also by the concentration of the available protons in the vicinity of Ni, hence Ni/HZSM-5 11.5 having the

highest concentration of Brønsted acid sites (Table 2) would have the highest [H] concentration. On the other hand, the result of phenol adsorption on Ni/HZSM-5 with different framework Si/Al ratios suggests that the higher TOF could also be partially attributed to the enrichment of phenol and the reaction intermediates in the pores of the more acidic zeolite. Considering that the reaction orders of a and b for adsorbed phenol and H were reported to be positive in the gas phase,²³ the enrichments of phenol and hydrogen would both positively influence the hydrogenation activity.

3.3 Hydrodeoxygenation of catechol

As Ni/HZSM-5 with the support framework Si/Al = 11.5 showed the highest catalytic activity in phenol hydrodeoxygenation, it was chosen to study the kinetics of a stepwise aqueous-phase conversion of substituted phenolic monomers. Catechol, *i.e.*, 1,2-dihydroxybenzene, was converted over this catalyst at 473 K in water (Fig. 5). In order to explore the complete reaction

network, a higher amount of catalyst was applied in comparison with phenol HDO. At the first stage of hydrodeoxygenation, aryl C–O bond hydrogenolysis and aromatic ring hydrogenation occurred in parallel. The latter reaction dominated, leading primarily to cyclohexane-1,2-diol with around 85% yield after 120 min (Fig. 5b). 2-Hydroxy cyclohexanone as a partial hydrogenation product of catechol was also observed in trace amounts (yield reached 2.4% in the first 20 minutes of reaction, and gradually consumed afterwards). The TOF for catechol hydrogenation on Ni was $809 \text{ mol}_{\text{catechol}} \text{ mol}_{\text{surf. Ni}}^{-1} \text{ h}^{-1}$ (accounting for contributions from both cyclohexane-1,2-diol and 2-hydroxy cyclohexanone), which was much lower than the Pd/C catalyzed rate ($\sim 3500 \text{ mol}_{\text{catechol}} \text{ mol}_{\text{surf. Pd}}^{-1} \text{ h}^{-1}$),⁹ in line with the weaker hydrogenation ability generally observed for Ni compared to Pd. On the other hand, substantial concentrations of phenol were detected as the primary product (at $t = 100 \text{ min}$, yield = 12%), suggesting that Ni catalyzed also direct hydrogenolysis of the $\text{C}_{\text{aryl}}\text{O}$ bond in cate-

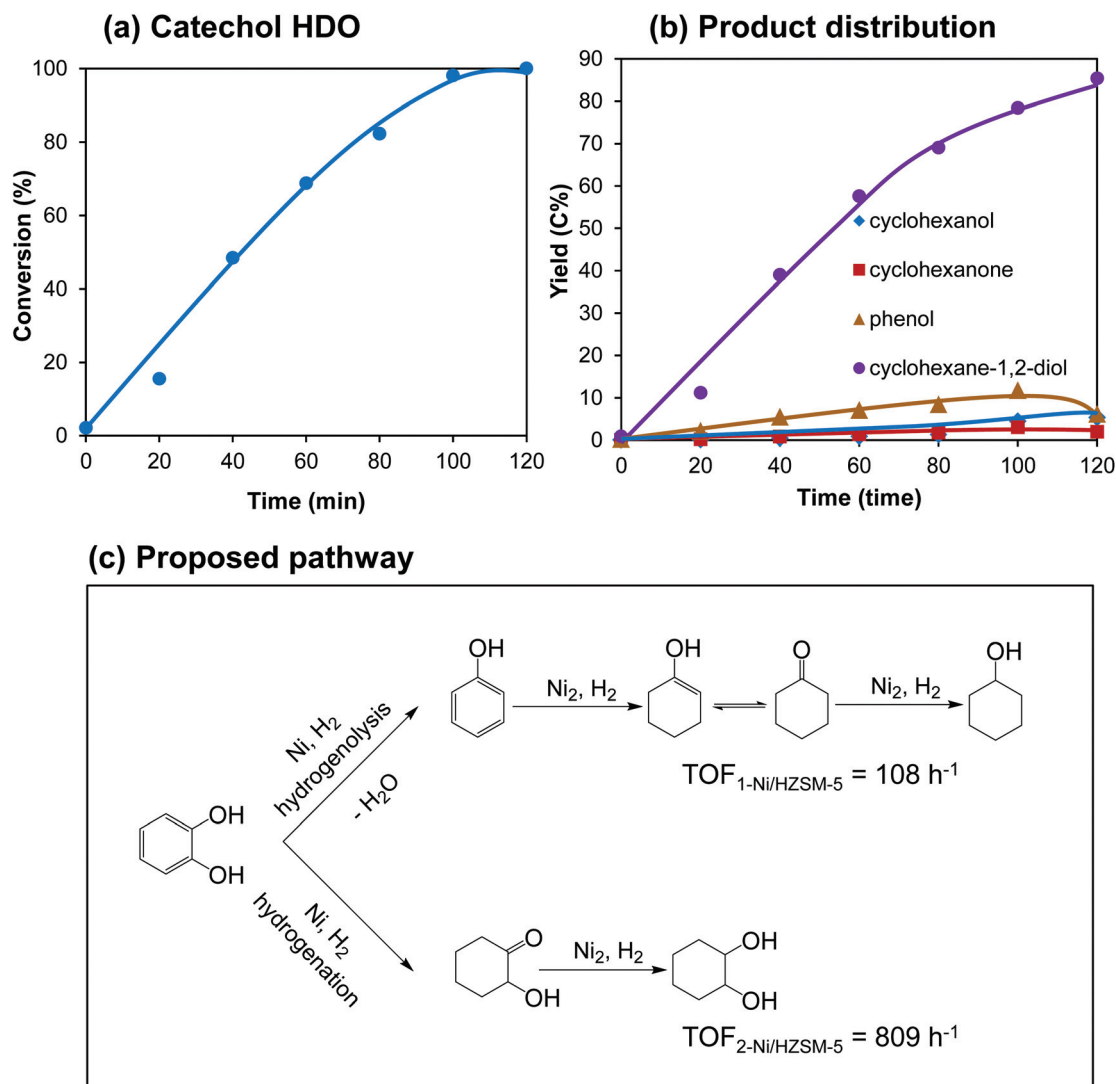


Fig. 5 Catechol hydrodeoxygenation over Ni/HZSM-5, (a) conversion, (b) product distribution, (c) proposed reaction pathway. Reaction conditions: 1.0 g catechol, 0.05 g Ni/HZSM-5, 473 K, 30 bar H_2 (ambient temperature), stirring at 700 rpm.

chol, as an alternative pathway.⁹ The formed phenol could be in turn gradually hydrodeoxygenated as proposed above. By comparison, with Pd/C as the catalyst, the rate of aromatic ring hydrogenation was orders of magnitude faster than that of hydrogenolysis. Thus, only the hydrogenation product was observed during catechol conversion on Pd/C.^{9,17a} It should be noted that benzene was not detected at any time during the conversion of catechol, and was also absent, when phenol was directly used as the reactant. This infers that the C–O bond cleavage of phenol is not favored on Ni in the aqueous phase under the reaction conditions applied, albeit Ni is efficient in the gas phase phenol hydrogenolysis.²⁴

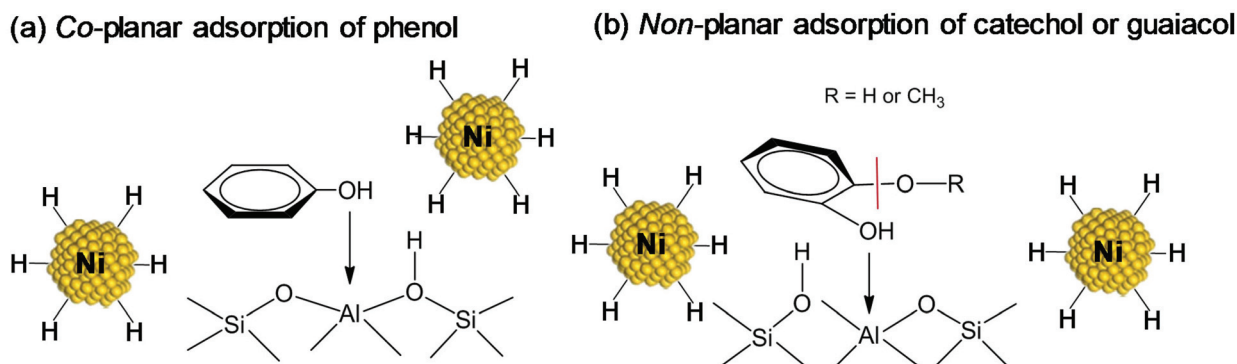
In summary, the C–O bond of catechol was directly cleaved by hydrogenolysis with a rate that was an eighth of the arene hydrogenation. The saturated diol produced could be further hydrodeoxygenated under more severe conditions. These results indicate that a much lower C–O hydrogenolysis barrier exists for catechol compared to phenol, which is attributed to the weaker C–O bond induced by electron donation from the adjacent –OH substituent²⁵ or the steric influence of the second *ortho*-substituted hydroxyl group in catechol.

As phenol tends to be adsorbed in a co-planar manner at the acidic surface (Scheme 2a),²⁶ hydrogenation is favored. The steric hindrance from the second –OH group in catechol, or the –OCH₃ group in guaiacol, leads preferentially to a non-planar adsorption mode. Consequently, hydrogenolysis is

more likely to take place on catechol and guaiacol (Scheme 2b).

As a mono-functional catalyst, HZSM-5 alone was inactive for catechol conversion (Table 5). While with the reference Ni/SiO₂, TOFs calculated for hydrogenolysis and hydrogenation were only 24 and 155 mol_{catechol} mol_{surf. Ni}⁻¹ h⁻¹, respectively (Table 5). This shows that hydrogenolysis and hydrogenation on mono-functional Ni/SiO₂ are much slower than on bifunctional Ni/HZSM-5, pointing again to the positive influences of support acidity on the Ni catalyzed steps. In analogy to the phenol hydrogenation discussed above, it is speculated that the acidic zeolite also enhances the adsorption of catechol, and provides abundant protons *via* zeolite Brønsted acid sites which are in the close vicinity of the metal.

Hydrodeoxygenation of cyclohexane-1,2-diol. Since *cis*-cyclohexane-1,2-diol was observed to be the main product from catechol hydrogenation, it was applied as the substrate to further investigate the C–O bond cleavage mechanism over Ni/HZSM-5. To overcome the higher C–O bond dissociation energy of the saturated alcohol, higher temperature (523 K) and catalyst to reactant ratio (1:0.2) were employed. Cyclohexane-1,2-diol, the major product from catechol hydrogenation, was applied in the study. 70% cyclohexane-1,2-diol was converted in 2 h at 523 K (Fig. 6a). Fig. 6b shows the main products formed during cyclohexane-1,2-diol hydrodeoxygenation,



Scheme 2 Adsorption of (a) phenol (co-planar mode) and (b) catechol/guaiacol (non-planar mode) on Ni/HZSM-5.

Table 5 Catechol hydrodeoxygenation over HZSM-5 or Ni/SiO₂ in separate experiments^a

Catalyst	Conv. (%)	Yield after 20 min (C%)						TOF ₁ ^b (h ⁻¹)	TOF ₂ ^c (h ⁻¹)
HZSM-5	—	—	—	—	—	—	—	—	
Ni/SiO ₂	31	—	0.05	0.20	3.8	0.37	26	24	155

^a Reaction conditions: 1 g catechol, 0.05 g catalyst, 473 K, 30 bar H₂ (ambient temperature), stirring at 700 rpm, 20 min reaction. ^b TOF₁ is defined as moles of catechol converted to hydrogenolysis products per mole of the surface Ni site per hour. ^c TOF₂ is defined as moles of catechol converted to hydrogenation products per mole of the surface Ni site per hour.

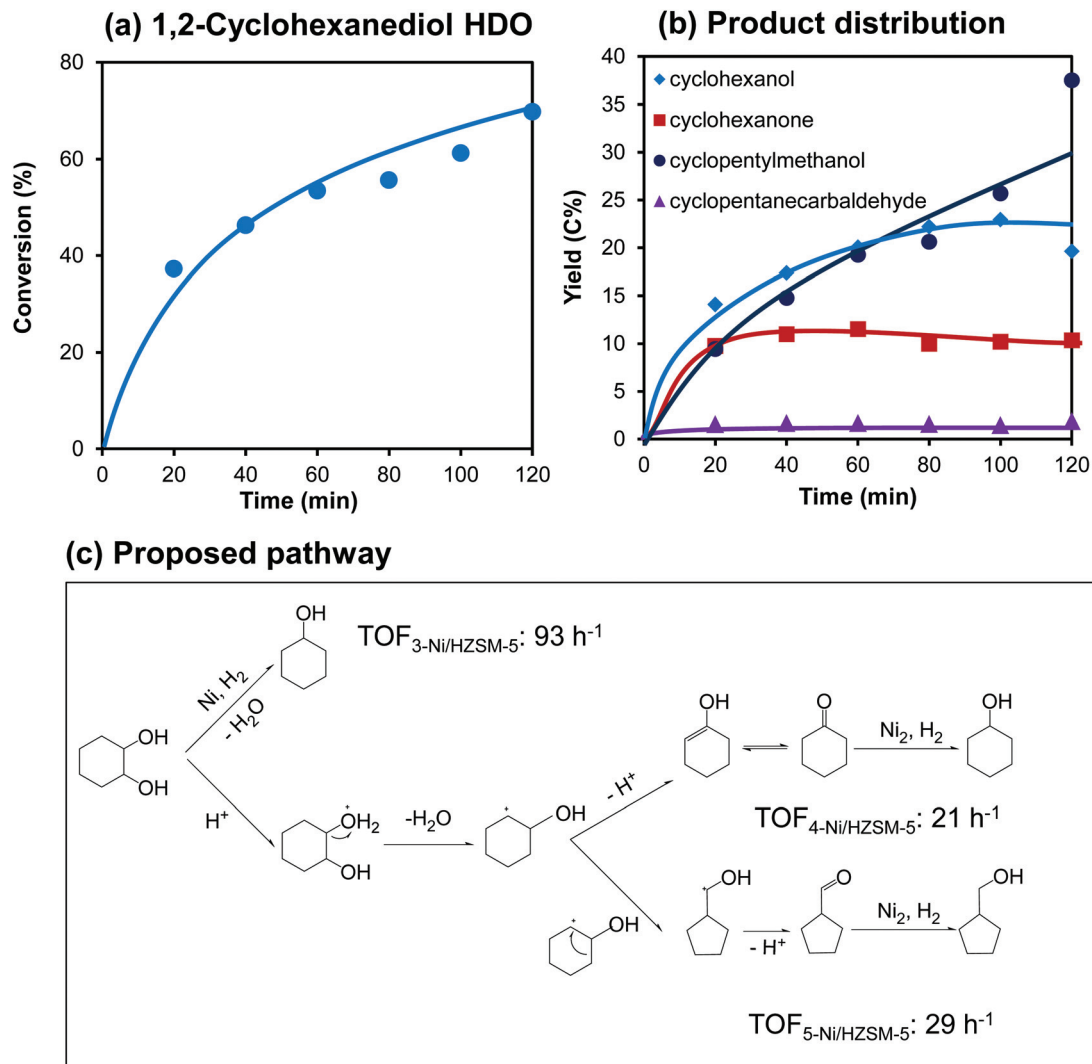


Fig. 6 Cyclohexane-1,2-diol hydrodeoxygenation over Ni/HZSM-5, (a) conversion, (b) product distribution, (c) proposed reaction pathway. Reaction conditions: 0.2 g cyclohexane-1,2-diol, 0.04 g Ni/HZSM-5, 523 K, 30 bar H₂ (ambient temperature), stirring at 700 rpm.

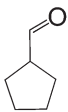
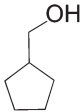
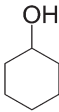
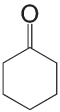
including cyclohexanone, cyclohexanol, and isomerized products of cyclopentylmethanol and cyclopentanecarbaldehyde.

Cyclohexanol could be formed either *via* direct hydrogenolysis of the C–O bond catalyzed by Ni or through a combination of acid catalyzed dehydration and Ni catalyzed alkene hydrogenation (Fig. 6c). Note that in order to calculate the initial TOF for each individual pathway, the concentration of primarily formed cyclohexanone was applied to determine the dehydration TOF₄, while TOF₃ (hydrogenolysis) was calculated based on the concentration of cyclohexanol, assuming that cyclohexanone hydrogenation is much slower than the dehydration of the saturated diol. Consequently, TOF₃ was slightly overestimated at 93 mol_{cyclohexane-1,2-diol} mol_{surf. Ni}⁻¹ h⁻¹, as the contribution of cyclohexanol from cyclohexanone hydrogenation could not be fully excluded. Apart from cyclohexanone and cyclohexanol, isomerized ketone and alcohol were also produced *via* acid catalyzed pinacol rearrangement in the presence of the acid catalyst (Fig. 6c).²⁷ The dehydration

route forming cyclohexanol had a TOF₄ of 21 mol_{cyclohexane-1,2-diol} mol_{BAS}⁻¹ h⁻¹, and the dehydration/isomerization pathway providing isomerized cyclopentyl methanol also reached a comparable initial TOF₅ of 29 mol_{cyclohexane-1,2-diol} mol_{BAS}⁻¹ h⁻¹ (Fig. 6c). Note that the C–O bond hydrogenolysis rate of cyclohexane-1,2-diol on Ni/HZSM-5 was lower than that of catechol at 473 K, leaving cyclohexane-1,2-diol almost unconverted at lower temperatures (Fig. 5b). This is related to both steric and electronic effects. The planar benzyl molecule with highly delocalized π orbitals facilitates higher adsorption constants of aromatic molecules,²⁸ in comparison with saturated cyclic compounds with less regular chair conformation and sp³ orbitals.

With mono-functional Ni/SiO₂ or HZSM-5, different product distributions in separate experiments were observed for cyclohexane-1,2-diol HDO (Table 6). HZSM-5 led to a highly selective dehydration, with direct dehydration of TOF₄ at 16 mol_{cyclohexane-1,2-diol} mol_{BAS}⁻¹ h⁻¹ and the dehydration/iso-

Table 6 1,2-Cyclohexanediol hydrodeoxygenation over mono-functional HZSM-5 or Ni/SiO₂^a

Catalyst	Conv. (%)	Yield after 2 h (C%)				TOF ₃ ^b (h ⁻¹)	TOF ₄ ^c (h ⁻¹)	TOF ₅ ^d (h ⁻¹)
								
HZSM-5	82	12	1.1	0.7	68	—	16	3.0
Ni/SiO ₂	68	2.7	18	20	27	11	—	—

^a Reaction conditions: 0.2 g 1,2-cyclohexanediol, 0.04 g catalyst, 523 K, 30 bar H₂ (ambient temperature), stirring at 700 rpm, 2 h reaction. ^b TOF₃ is defined as moles of 1,2-cyclohexanediol converted to hydrogenolysis products per mole of the surface Ni site per hour. ^c TOF₄ is defined as moles of 1,2-cyclohexanediol converted to dehydration products per mole of the Brønsted acid site per hour. ^d TOF₅ is defined as moles of 1,2-cyclohexanediol converted to dehydration-isomerization products per mole of the Brønsted acid site per hour.

merization of 3.0 mol_{cyclohexane-1,2-diol} mol_{BAS}⁻¹ h⁻¹. The isomerization rate on HZSM-5 was one magnitude lower than that on Ni/HZSM-5 (3 *versus* 29 h⁻¹), suggesting that Ni helps to facilitate the carbocation rearrangement at the acid sites. On the other hand, the hydrogenolysis activity with Ni/SiO₂ (11 h⁻¹) was about nine times lower than that of Ni/HZSM-5 (93 h⁻¹), demonstrating again the synergistic effects between Brønsted acid and Ni sites for enhancing the catalytic activity of the metal. Note that some isomers of cyclopentylmethanol and aldehyde were also observed with the Ni/SiO₂ catalyzed reaction, probably formed due to the presence of the hydronium ions originating from hot liquid water at 523 K (pH = 5.5).²⁹

In summary, at 523 K the C–O bond cleavage of cyclohexane-1,2-diol was concluded to proceed with parallel routes of direct Ni-catalyzed hydrogenolysis and acid-catalyzed dehydration, reaching an initial TOF of approximately one sixth of that observed with catechol, even at elevated the temperature.

3.4 Hydrodeoxygenation of guaiacol

Guaiacol, *i.e.*, 2-methoxyphenol with adjacent –OH and –OCH₃ groups at the aromatic ring, is the most abundant phenolic monomer from lignin depolymerization.³⁰ Hydrodeoxygenation of guaiacol at 473 K led to the formation of a wide range of products including cyclohexanol, cyclohexanone, aromatics, and methanol (Fig. 7b). Similarly to catechol, hydrogenation and hydrogenolysis occurred in parallel on Ni/HZSM-5. The TOF of guaiacol hydrogenation only reached 21 mol_{guaiacol} mol_{surf. Ni}⁻¹ h⁻¹ (Fig. 7c), which was a magnitude slower than the hydrogenation of catechol or phenol. The steric influence of the *ortho*-substituted sp³ methoxy group is concluded to make the co-planar adsorption of the aromatic ring more difficult compared to phenol and catechol, and hence, causes the low hydrogenation activity. This trend was also observed for the Pd catalyzed hydrodeoxygenation of phenolic monomers in the aqueous phase.⁹

The structure of guaiacol contains three types of C–O bonds, *i.e.*, C_(sp³)–OAr, C_(sp²)–OMe, and C_(sp²)–OH (see Fig. 8), with the respective bond dissociation energy (BDE) of 262–276, 409–421, and 466 kJ mol⁻¹. From the BDE point of view, the

energy barrier of C_(sp²)–OH bond scission is the highest, and this corresponds well with our result in which the yield of methoxybenzene was lower than 0.1% (Fig. 7b). Demethylation *via* C_(sp³)–OAr bond scission is more favorable compared with demethoxylation *via* cleavage of the C_(sp²)–OMe bond in terms of bond strength. For instance, sulfide catalysts usually lead to the hydrogenolysis of guaiacol through demethylation forming catechol.⁷ Surprisingly, only a trace amount of catechol was observed in the present case, while phenol (including cyclohexanone, cyclohexanol, and cyclohexane as subsequent products) was the dominant primary product (at *t* = 20 min, selectivity = 78 C%). Moreover, the fact that methanol was formed at a yield of around 1/6 of phenol, together with the absence of methane in the gas phase confirmed the dominant pathway of direct demethoxylation *via* the cleavage of the C_{aryl}–OMe bond, and the demethylation route on Ni/HZSM-5 was excluded under the present reaction conditions. The demethoxylation pathway was also observed for guaiacol hydrodeoxygenation at 543–573 K in the gas phase when Co promoted transition metal sulfide^{31a} or carbon supported CoMo catalysts^{31b} were used. The high preference for demethoxylation over demethylation is speculated to be caused by the steric constraints, *i.e.*, the C_{aryl}–OMe bond approaches the Ni surface more easily.

In summary, hydrogenolysis is faster than hydrogenation for guaiacol hydrodeoxygenation, with a ratio of 3 : 1. This is in contrast to catechol conversion, possibly due to the more pronounced steric impact of the sp³ hybrid Me–OAr orbital than the sp² hybrid C_{aryl}–OH orbital.

Employing HZSM-5 alone yielded only 0.8% catechol *via* guaiacol hydrolysis at 473 K (Table 7). This suggests again that hydrolysis of methoxy groups with acid sites is a negligible pathway for guaiacol conversion under the selected conditions. Thus, Ni is shown to be the active site.

Remarkably also in this case, the mono-functional Ni/SiO₂ led to much lower hydrogenation and hydrogenolysis TOFs than Ni/HZSM-5; the latter reached a TOF₇ (hydrogenation) of 21 *versus* 6.2 h⁻¹ and a TOF₆ (hydrogenolysis) of 62 *versus* 14 h⁻¹ (Table 7), respectively; in perfect agreement with the results of catechol conversion. The presence of support acidity pronouncedly enhances the rates of Ni-catalyzed steps; this

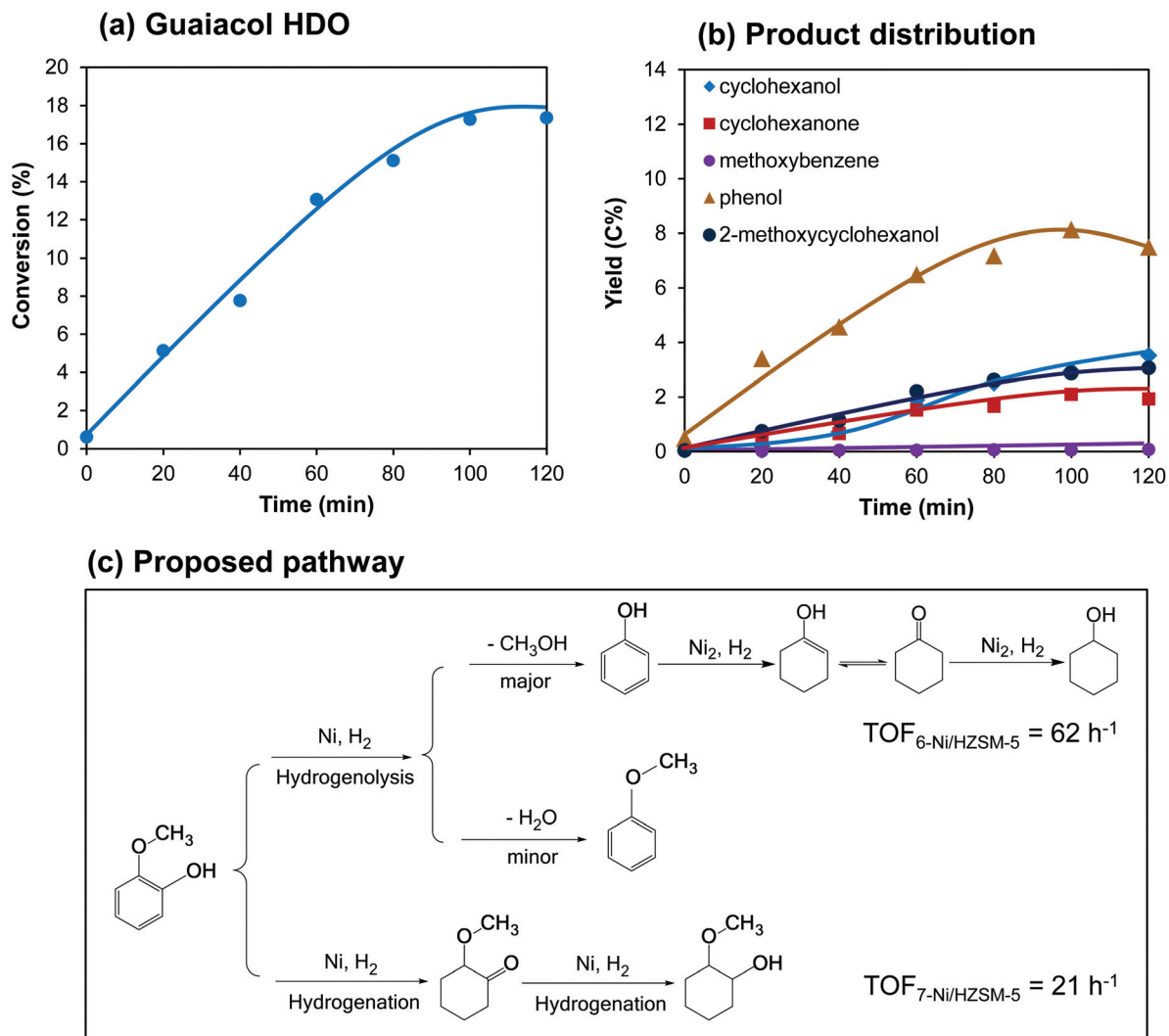


Fig. 7 Guaiacol hydrodeoxygenation over Ni/HZSM-5, (a) conversion, (b) product distribution, (c) proposed reaction pathway. Reaction conditions: 1 g guaiacol, 0.05 g Ni/HZSM-5, 473 K, 30 bar H₂ (ambient temperature), stirring at 700 rpm.

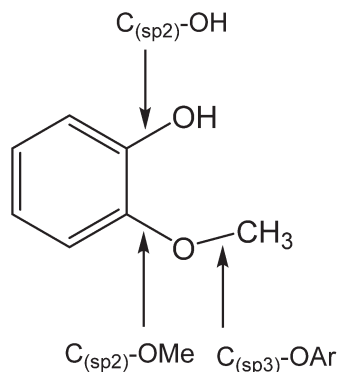
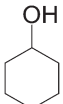
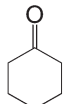
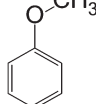
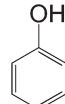
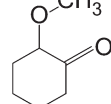
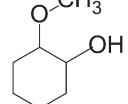
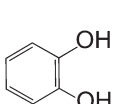


Fig. 8 Structure of guaiacol.

implies again that protons might be directly involved in the catalytic processes in a way that has been suggested for the enhanced rate of hydrogen oxidation in organometallic complexes.^{22c}

Hydrodeoxygenation of 2-methoxycyclohexanol. Although both *cis*- and *trans*- forms of 2-methoxycyclohexanol were intermediately formed from guaiacol hydrogenation, the *trans* conformer dominated and thus it was selected to explore the further hydrodeoxygenation (Fig. 9a). At 523 K, 2-methoxycyclohexanol was shown to be readily converted to cyclohexanol, cyclohexanone and their isomers over Ni/HZSM-5 (Fig. 9b) similarly to the reaction of cyclohexane-1,2-diol. However, in the case of 2-methoxycyclohexanol, isomerized cyclopentyl-methanol was primarily formed (at $t = 2$ h, selectivity > 80 C%), unlike the conversion of cyclohexane-1,2-diol, in which direct dehydration (TOF = 21 h⁻¹) and dehydration/isomerization (TOF = 29 h⁻¹) proceeded in parallel pathways with nearly equal contribution. This implies that in spite of the similar final products, hydrodeoxygenation of 2-methoxycyclohexanol passes through a different transition state compared to the one proposed for cyclohexane-diol (Fig. 9c). On the other hand, even increasing both the temperature and the amount

Table 7 Guaiacol hydrodeoxygenation over mono-functional HZSM-5 or Ni/SiO₂^a

Catalyst	Conv. (%)	Yield after 40 min (C%)							TOF ₆ ^b (h ⁻¹)	TOF ₇ ^c (h ⁻¹)
										
HZSM-5	0.79	—	—	—	—	—	—	0.79	—	—
Ni/SiO ₂	13	1.9	1.3	0.04	5.9	0.86	3.0	—	14	6.2

^a Reaction conditions: 1 g guaiacol, 0.05 g catalyst, 473 K, 30 bar H₂ (ambient temperature), stirring at 700 rpm, 40 minute reaction. ^b TOF₆ is defined as moles of guaiacol converted to hydrogenolysis products per mole of the surface Ni site per hour. ^c TOF₇ is defined as moles of guaiacol converted to hydrogenation products per mole of the surface Ni site per hour.

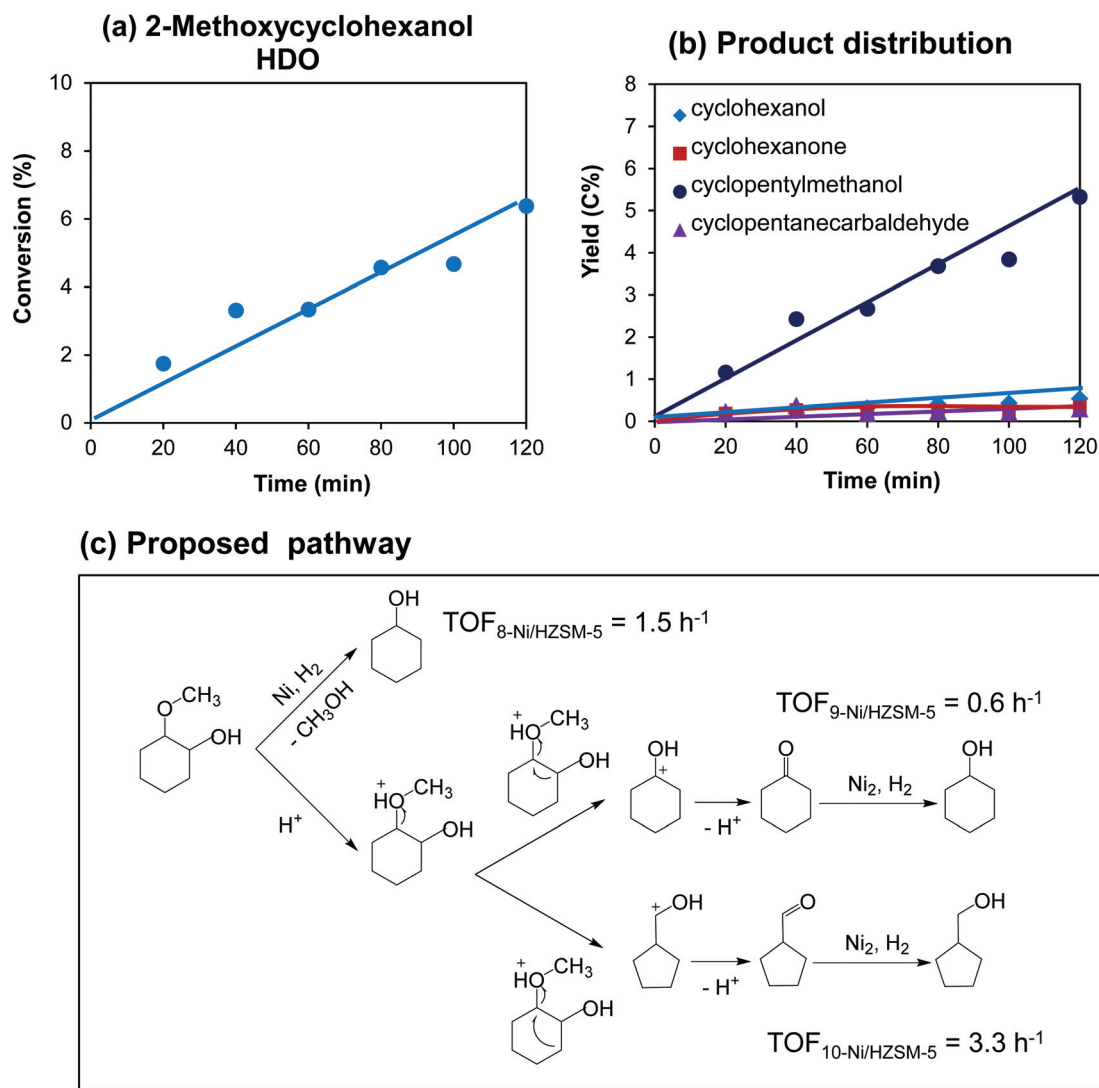
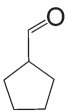
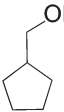
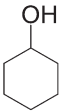
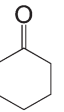
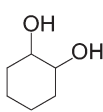


Fig. 9 2-Methoxycyclohexanol hydrodeoxygenation over Ni/HZSM-5, (a) conversion, (b) product distribution, (c) proposed reaction pathway. Reaction conditions: 0.2 g 2-methoxycyclohexanol, 0.04 g Ni/HZSM-5, 523 K, 30 bar H₂ (ambient temperature), stirring at 700 rpm.

of catalyst, the conversion of 2-methoxycyclohexanol over Ni/HZSM-5 (6.4%) was about three times lower than guaiacol conversion (18%) at 473 K after 2 h. This is probably resulted

from the steric and electronic influences of the saturated cyclic ring as discussed for cyclohexane-diol. 2-Methoxycyclohexanol was also much less active than the saturated diol, with an

Table 8 2-Methoxycyclohexanol hydrodeoxygenation over mono-functional HZSM-5 or Ni/SiO₂^a

Catalyst	Conv. (%)	Yield after 2 h (C%)					TOF ₈ ^b (h ⁻¹)	TOF ₉ ^c (h ⁻¹)	TOF ₁₀ ^d (h ⁻¹)
									
HZSM-5	8.3	7.1	—	—	0.90	0.34	—	0.8	3.9
Ni/SiO ₂	5.3	0.5	4.0	0.54	0.29	—	0.5	—	—

^a Reaction conditions: 0.2 g 2-methoxycyclohexanol, 0.04 g catalyst, 523 K, 30 bar H₂ (ambient temperature), stirring at 700 rpm, 2 h reaction.

^b TOF₈ is defined as moles of 2-methoxycyclohexanol converted to hydrogenolysis products per mole of the surface Ni site per hour. ^c TOF₉ is defined as moles of 2-methoxycyclohexanol converted to dehydration products per mole of the Brønsted acid site per hour. ^d TOF₁₀ is defined as moles of 2-methoxycyclohexanol converted to dehydration–isomerization products per mole of the Brønsted acid site per hour.

initial rate of conversion of 6.4 h⁻¹ compared to 143 h⁻¹. Structural influences of the *ortho*-substituted –OCH₃ group should have accounted for the observed low activity.

The kinetics of applying solely HZSM-5 or Ni/SiO₂ was investigated with 2-methoxycyclohexanol at 523 K in separate experiments (Table 8). HZSM-5 alone catalyzed sequential hydrolysis and dehydration of 2-methoxycyclohexanol, with TOF₉ (towards cyclohexanone) of 0.8 h⁻¹ and TOF₁₀ (towards cyclopentane carbaldehyde) of 3.9 h⁻¹. This shows that the catalytic function of HZSM-5 is quite similar to that of the acid sites in Ni/HZSM-5 for 2-methoxycyclohexanol conversion. Low concentrations of cyclohexane-diol were detected, while this product was absent with Ni/HZSM-5 catalyzed reactions. This is attributed to the absence of the metal-catalyzed hydrogenolysis of cyclohexane-diol, as its consumption rate through hydrogenolysis is relatively fast (TOF = 93 h⁻¹, Fig. 6c) in comparison with its formation rate *via* hydrolysis. With the metal function only (Ni/SiO₂), the hydrogenolysis activity towards the formation of cyclohexanol (TOF: 0.5 h⁻¹) was slower than that catalyzed by Ni/HZSM-5 (TOF: 1.5 h⁻¹) (Fig. 9c), confirming again the enhanced activity of Ni in the presence of Brønsted acid sites. Some dehydration products were also observed, which were catalyzed by the hydronium ions originated from hot liquid water at 523 K as discussed above.

3.5 Overall hydrodeoxygenation pathways and rates of conversion of phenolic monomers

The activities and reaction pathways for cleaving the C–O bonds in phenol, catechol, and guaiacol over mono- or dual-functional Ni and HZSM-5 are summarized in Table 9. Under selected conditions with Ni/HZSM-5, phenol was hydrogenated to cyclohexanol in the first stage, and the C–O bond of cyclohexanol was subsequently cleaved by dehydration, which is similar to Pd/C–H₃PO₄ catalyzed phenol hydrodeoxygenation.⁹ However, with the adjacent –OH or –OCH₃ functional group attached to the *ortho* position of the phenolic ring, the reaction pathways for converting catechol and guaiacol change.

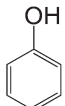
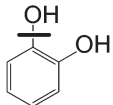
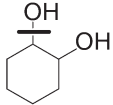
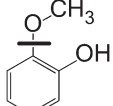
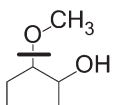
Catechol was hydrogenated to cyclohexane-1,2-diol (major) and hydrogenolyzed to phenol (minor) in parallel routes over Ni/HZSM-5. Subsequently, phenol was hydrodeoxygenated following the conventional hydrogenation–dehydration route,

whereas cyclohexane-1,2-diol was further converted through either dehydration or hydrogenolysis to cleave the aliphatic C–O bonds. Guaiacol, however, was hydrogenolyzed *via* demethoxylation of the C_{aryl}–OMe bond as the dominant route, forming phenol as the major primary product. The remaining fully hydrogenated 2-methoxycyclohexanol was converted either through cleavage of the C_{alkyl}–OMe bond on Ni forming methanol and cyclohexanol, or *via* acid mediated pathways toward the final formation of cyclohexanol and cyclopentylmethanol. The proposed reaction networks of catechol and guaiacol differ from the Pd-acid catalyzed reaction pathways, in which the cleavage of the C_{aryl}–O bond starts *via* full arene hydrogenation on Pd followed by C_{aliphatic}–O bond scission through acid catalyzed dehydration or hydrolysis.⁹ This indicates that the Pd catalyzed hydrogenation rate is significantly higher than the hydrogenolysis rate, whereas Ni is a better hydrogenolysis catalyst. The proposed mechanism is also different from the sole C–O bond hydrogenolysis pathway by sulfide transition metal catalysts in the gas phase.⁷

Phenolic monomers are generally more active than the corresponding fully hydrogenated intermediates. For example, the hydrogenation and hydrogenolysis rates of catechol were 809 and 108 h⁻¹ on Ni/HZSM-5 at 473 K, respectively; while the hydrogenolysis of cyclohexane-diol was only 93 h⁻¹ even at an elevated temperature of 523 K (Table 9, entries 2 and 3). Similarly, the hydrogenolysis rate of 2-methoxycyclohexanol was a magnitude lower than that of guaiacol on Ni/HZSM-5 (Table 9, entries 4 and 5). Again, the observed differences in reactivity are attributed to both steric and electronic constraints to cleave the C–O bond at the saturated ring. These results are of great importance to guide the lignin depolymerization and the subsequent upgrading processes, *i.e.*, direct hydrogenolysis of C_{aryl}–OR is much easier than hydrogenolysis of the respective C_{aliphatic}–OR.

The results summarized in Table 9 show clearly that the presence of support acidity has a positive impact on the activities of Ni catalyzed steps. For instance, the TOF of phenol hydrogenation was 769 h⁻¹ over Ni/HZSM-5, and 127 h⁻¹ for Ni/SiO₂. Similarly, the rates of hydrogenation and hydrogenolysis of catechol were 809 and 108 h⁻¹ on Ni/HZSM-5, while Ni/SiO₂ only achieved TOFs of 155 and 24 h⁻¹ under the same

Table 9 C–O bond cleavage pathways for phenolic monomers over Ni and HZSM-5 sites

Entry	Reactant	C–O cleavage pathway	Active center	TOF (h ⁻¹)		
				Ni/HZSM-5	HZSM-5	Ni/SiO ₂
1		Hydrogenation–dehydration	Ni ^a	769	—	127
2		Hydrogenation Hydrogenolysis	Ni ^a	809	—	155
			Ni ^a	108	—	24
3		Hydrogenolysis Dehydration	Ni ^b	93	—	11
			HZSM-5 ^b	50	19	—
4		Hydrogenation Hydrogenolysis	Ni ^a	21	—	6.2
			Ni ^a	62	—	14
5		Hydrogenolysis Demethoxylation	Ni ^b	1.5	—	0.5
			HZSM-5 ^b	3.9	4.7	—

^a Temperature: 473 K. ^b Temperature: 523 K.

conditions. Similarly, rates of guaiacol HDO were much higher with Ni/HZSM-5 than with Ni/SiO₂. The acid support is on the one hand enhancing the strength of adsorption of the phenolic monomers. On the other hand, the present case might be a remarkable analogy to the rate enhancements observed for hydrogen oxidation by organometallic complexes, where Brønsted acid sites are speculated to be directly involved in the hydrogenation reaction. It highlights the importance of synergistic effects of proximal metal and acid sites in a bifunctional catalyst where a fraction of Ni being catalytically active is present in the vicinity of the zeolite acid sites.

4. Conclusions

The mechanisms for C–O bond cleavage in phenol, catechol, and guaiacol have been investigated in the aqueous phase. Remarkable synergistic effects with Ni supported on and in HZSM-5 pores are described. Phenol is hydrodeoxygenated on Ni/HZSM-5 through primary hydrogenation to cyclohexanol, and the subsequent dehydration of cyclohexanol, followed by cyclohexene hydrogenation, similarly with the conversions catalyzed by Pd in the presence of aqueous mineral acids. Catechol is converted by parallel hydrogenation (forming cyclohexane-1,2-ol, 89%) and hydrogenolysis (forming phenol, 11%) over Ni/HZSM-5. The C–O bond of cyclohexane-1,2-diol is readily cleaved either by direct hydrogenolysis over Ni (major route), or by further dehydration and pinacol rearrangement on acid sites (minor route). For the

hydrodeoxygenation of guaiacol, hydrogenation (25%) and hydrogenolysis (75%) pathways proceed in parallel, producing 2-methoxycyclohexanol and phenol as primary products. 2-Methoxycyclohexanol can be in turn either hydrogenolyzed to cyclohexanol (minor route) by Ni, or converted *via* demethoxylation and rearrangement steps (major route) catalyzed by acid sites.

The catalytic conversions of saturated cyclic alcohols are much slower than those of their respective phenolic monomers, suggesting that the cleavage of C–O bonds attached to the saturated ring is more difficult. This is attributed to the difference in hybridization, which imposes a steric constraint for the active metal center to approach the C–O bonds. The Ni/HZSM-5 for hydrodeoxygenation of phenolic monomers utilizes both Ni and Brønsted acid functions to seamlessly catalyze the cascade reactions, more importantly, the acid sites in the vicinity of metal lead to markedly promoted rates in hydrogenation and hydrogenolysis. The synergistic effect contributes to prominent rate enhancement compared to Ni/SiO₂ catalysts. This increase is tentatively attributed to the combination of a higher concentration of the reacting substrate and an additional delivery of hydrogen through protons from the nearby strong Brønsted acid sites.

Acknowledgements

W. S. gratefully acknowledges support from the Graduate School (Faculty Graduate Center of Chemistry) of the

Technische Universität München and the Elitenetzwerk Bayern (Graduate School NanoCat). J.A.L acknowledges the partial support from the US Department of Energy, Office of Basic Energy Sciences, Division of Chemical Sciences, Geosciences & Biosciences. Pacific Northwest National Laboratory (PNNL) is a multi-program national laboratory operated for DOE by Battelle.

References

- (a) F. S. Chakar and A. Ragauskas, *J. Ind. Crops Prod.*, 2004, **20**, 131; (b) J. Zakzeski, P. C. A. Bruijninx, A. L. Jongerius and B. M. Weckhuysen, *Chem. Rev.*, 2010, **110**, 3552.
- M. Stöcker, *Angew. Chem., Int. Ed.*, 2008, **47**, 9200.
- G. W. Huber and A. Corma, *Angew. Chem., Int. Ed.*, 2007, **46**, 7184.
- E. Furimsky, *Appl. Catal., A*, 2000, **199**, 147.
- S. W. Benson, *Thermochemical Kinetics*, Wiley, New York, 1968.
- (a) M. J. Girgis and B. C. Gates, *Ind. Eng. Chem. Res.*, 1991, **30**, 202; (b) H. Topsøe, B. S. Clausen and F. E. Massoth, *Hydrotreating Catalysis Science and Technology*, Springer, Berlin, 1996.
- (a) M. Ferrari, A. Centeno, C. Lahousse, R. Maggi, P. Grange and B. Delmon, *Am. Chem. Soc. Div. Pet. Chem. Prepr.*, 1998, **43**, 94; (b) J. B. Bredenberg, M. Huuska and P. Toropainen, *J. Catal.*, 1989, **120**, 401; (c) E. Laurent and B. Delmon, *Appl. Catal.*, 1994, **109**, 97.
- A. Centeno, E. Laurent and B. Delmon, *J. Catal.*, 1995, **154**, 288.
- C. Zhao, J. He, A. A. Lemonidou, X. Li and J. A. Lercher, *J. Catal.*, 2011, **280**, 8.
- C. Zhao and J. A. Lercher, *Angew. Chem., Int. Ed.*, 2012, **51**, 5935.
- R. Nares, J. Ramírez, A. Gutiérrez-Alejandre, C. Louis and T. Klimova, *J. Phys. Chem. B*, 2002, **106**, 13287.
- (a) B. C. Lippens, B. G. Linsen and J. H. d. Boer, *J. Catal.*, 1964, **3**, 32; (b) W. D. Harkins and G. Jura, *J. Am. Chem. Soc.*, 1944, **66**, 1366.
- P. Burattin, M. Che and C. Louis, *J. Phys. Chem. B*, 1998, **102**, 2722.
- (a) W. Song, C. Zhao and J. A. Lercher, *Chem. – Eur. J.*, 2013, **19**, 9833; (b) C. Zhao, T. Brück and J. A. Lercher, *Green Chem.*, 2013, **15**, 1720.
- (a) K. Hadjiivanov, M. Mihaylov, D. Klissurski, P. Stefanov, N. Abadjieva, E. Vassileva and L. Mintchev, *J. Catal.*, 1999, **185**, 314; (b) A. G. Sault, C. H. F. Peden and E. P. Boespflug, *J. Phys. Chem.*, 1994, **98**, 1652; (c) J. Leglise, A. Janin, J. C. Lavalley and D. Cornet, *J. Catal.*, 1988, **114**, 388; (d) L. Bonneviot, F. Cai, M. Che, K. Kermarec, O. Legendre, C. Lepetit and D. Olivier, *J. Phys. Chem.*, 1987, **91**, 5912; (e) J. B. Peri, *J. Catal.*, 1984, **86**, 84.
- (a) P. Burattin, M. Che and C. Louis, *J. Phys. Chem. B*, 1997, **101**, 7060; (b) P. Burattin, M. Che and C. Louis, *J. Phys. Chem. B*, 1999, **103**, 6171; (c) P. Burattin, M. Che and C. Louis, *J. Phys. Chem. B*, 2000, **104**, 10482.
- (a) C. Zhao, Y. Kou, A. A. Lemonidou, X. Li and J. A. Lercher, *Angew. Chem., Int. Ed.*, 2009, **48**, 3987; (b) C. Zhao and J. A. Lercher, *ChemCatChem*, 2012, **4**, 64.
- A. Popov, E. Kondratieva, J. M. Goupil, L. Mariey, P. Bazin, J.-P. Gilson, A. Travert and F. Maugé, *J. Phys. Chem. C*, 2010, **114**, 15661.
- C. Zhao, D. M. Camaioni and J. A. Lercher, *J. Catal.*, 2012, **288**, 92.
- A. Jentys, R. R. Mukti, H. Tanaka and J. A. Lercher, *Microporous Mesoporous Mater.*, 2006, **90**, 284.
- (a) G. Larsen and G. L. Haller, *Catal. Lett.*, 1989, **3**, 103; (b) Z. Karpiński, S. N. Gandhi and W. M. H. Sachtler, *J. Catal.*, 1993, **141**, 337; (c) B. L. Mojet, J. T. Miller, D. E. Ramaker and D. C. Koningsberger, *J. Catal.*, 1999, **186**, 373.
- (a) M. R. Dubois and D. L. Dubois, *Acc. Chem. Res.*, 2009, **42**, 1974; (b) M. O' Hagan, W. J. Shaw, S. Raugei, S. Chen, J. Y. Yang, U. J. Kilgore, D. L. Dubois and R. M. Bullock, *J. Am. Chem. Soc.*, 2011, **133**, 14301; (c) M. O'Hagan, M. H. Ho, J. Y. Yang, A. M. Appel, M. Rakowski DuBois, S. Raugei, W. J. Shaw, D. L. DuBois and R. M. Bullock, *J. Am. Chem. Soc.*, 2012, **134**, 19409; (d) T. Liu, D. L. DuBois and R. M. Bullock, *Nat. Chem.*, 2013, **5**, 228.
- N. Mahata, K. V. Raghavan and V. Vishwanathan, *Catal. Today*, 1999, **49**, 65.
- (a) E.-J. Shin and M. A. Keane, *Ind. Eng. Chem. Res.*, 2000, **39**, 883; (b) J. B. Bredenberg, M. Huuska, J. Rätty and M. Korpio, *J. Catal.*, 1982, **77**, 242.
- E.-J. Shin and M. A. Keane, *J. Catal.*, 1998, **173**, 450.
- G. Neri, A. M. Viso, A. Donato, C. Milone, M. Malentacchi and G. Gubitosa, *Appl. Catal., A*, 1994, **110**, 49.
- T. Xu and J. F. Haw, *J. Am. Chem. Soc.*, 1994, **116**, 7753.
- C. Zhao, Y. Yu, A. Jentys and J. A. Lercher, *Appl. Catal., B*, 2013, **132–133**, 282.
- G. C. Akerlof and H. I. Oshry, *J. Am. Chem. Soc.*, 1950, **72**, 2844.
- V. M. Roberts, V. Stein, T. Reiner, A. A. Lemonidou and J. A. Lercher, *Chem. – Eur. J.*, 2011, **17**, 5939.
- (a) V. N. Bui, D. Laurenti, P. Afanasiev and C. Geantet, *Appl. Catal., B*, 2011, **101**, 239; (b) M. Ferrari, R. Maggi, B. Deomon and P. Grange, *J. Catal.*, 2001, **198**, 47.